PERGAMON

Engineering Fracture Mechanics 68 (2001) 129–147

Engineering Fracture Mechanics

www.elsevier.com/locate/engfracmech

Effect of load ratio and maximum stress intensity on the fatigue threshold in Ti–6Al–4V

B.L. Boyce, R.O. Ritchie *

Department of Materials Science and Engineering, University of California, Berkeley, CA 94720-1760, USA

Received 14 February 2000; received in revised form 30 September 2000; accepted 2 October 2000

Abstract

There has been a renewed interest of late in the mechanisms responsible for the influence of the load ratio, R, and the maximum stress intensity, K_{max}, on the threshold for fatigue-crack growth, ΔK_{th}. While mechanistic explanations in the past have largely focused on the role of crack closure, it is certainly not the only mechanism by which K_{max} influences ΔK_{th}. In this work, we examine the effect of a wide range of loading frequencies ($\nu = 50$–1000 Hz) and load ratios ($R = 0.10$–0.95) on fatigue-crack propagation and threshold behavior in a Ti–6Al–4V turbine blade alloy consisting of $\sim$60 vol% primary-α and $\sim$40 vol% lamellar $\alpha + \beta$. The data presented in this paper indicate that at K_{max} values above 6 MPa$\sqrt{m}$ ($R > 0.5$), where macroscopic crack closure is no longer detected in this alloy, ΔK_{th} decreases approximately linearly with increasing K_{max}. This result is discussed in terms of possible mechanistic explanations, including sustained-load cracking, microscopic near-tip closure, and static fracture modes, based on considerations of experimental evidence from both the current study and the literature. © 2000 Published by Elsevier Science Ltd.

Keywords: Titanium alloys; Ti–6Al–4V; Fatigue threshold; Load ratio; Crack closure; Sustained-load cracking

1. Introduction

The influence of load ratio, [1] R, on fatigue-crack propagation rates has been widely studied from both experimental (e.g. Refs. [1–6]) and analytical (e.g. Refs. [7,8]) viewpoints. Almost without exception, an increase in load ratio results in an increase in fatigue-crack propagation rate at a given applied cyclic stress-intensity, ΔK. Equivalently, the observed threshold stress-intensity range for fatigue-crack propagation, ΔK_{th}, decreases as the (positive) load ratio is increased. Mechanistic explanations for such behavior have focused on (a) the presence of crack closure at low values of the minimum stress intensity, K_{min} [1] or (b) the presence of static fracture modes as the maximum stress intensity, K_{max}, approaches the fracture toughness, K_{Ic} [9].

* Corresponding author. Tel.: +1-510-486-5798; fax: +1-510-486-4995.

E-mail address: roritchie@lbl.gov (R.O. Ritchie).

[1] Load ratio, R, is defined under fatigue loading conditions as the minimum applied load divided by the maximum applied load for any given loading cycle.

0013-7944/01/$ - see front matter © 2000 Published by Elsevier Science Ltd.
PII: S0013-7944(00)00099-0

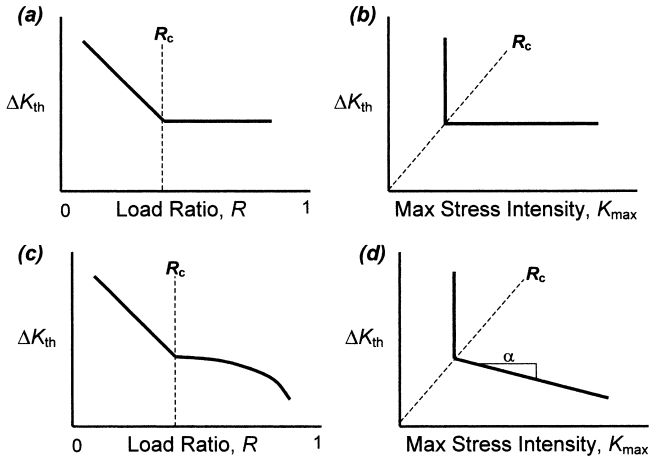

Fig. 1. (a) A "classic" representation of the influence of the load ratio, R, on the fatigue threshold, ΔK_{th}. (b) A transformation into coordinates of $(K_{max}, \Delta K_{th})$. (c) Many data sets, however, exhibit decreasing threshold even beyond the transition, $R > R_c$. (d) The variation of ΔK_{th} with K_{max} is shown here as approximately linear with slope, α.

A common conception of the variation in the fatigue threshold with load ratio is shown in Fig. 1a. Schmidt and Paris [1] rationalized this behavior solely on the basis of the crack closure concept. Assuming that both the closure-corrected effective fatigue threshold, $\Delta K_{eff,th}$ and the closure stress intensity, K_{cl}, are *not* affected by load ratio, then there exists some critical load ratio, R_c at which $K_{min} = K_{cl}$, such that:

$$\Delta K_{eff,th} = \begin{cases} K_{max,th} - K_{cl} < \Delta K_{th}, & \text{if } R < R_c \ (K_{min,th} < K_{cl}), \\ K_{max,th} - K_{min,th} = \Delta K_{th}, & \text{if } R > R_c \ (K_{min,th} > K_{cl}). \end{cases} \quad (1)$$

Under these conditions, the maximum stress intensity at threshold, $K_{max,th}$, is independent of R below R_c and the threshold stress-intensity range, ΔK_{th}, is independent of R above R_c. Plotted as $K_{max,th}$ versus ΔK_{th}, this transition manifests itself as a distinct 'L' shape, as shown in Fig. 1b, highlighting that the value of ΔK_{th} is independent of K_{max} when $R > R_c$ where global closure is no longer effective. As a first approximation, the Schmidt and Paris analysis seems to work moderately well, with many data sets showing this transition at load ratios similar to the critical load ratio condition, R_c, at which point $K_{min} = K_{cl}$.

This behavior, however, is not universal, as shown by the compilation of data presented in Fig. 2. In most cases, the value of ΔK_{th} is *not* invariant at $R > R_c$, but rather ΔK_{th} decreases with increasing R (Fig. 1c and d), implying that either the Schmidt and Paris model is not properly described at $R > R_c$, or that there are additional mechanisms acting *in concert*. It is this variation in ΔK_{th} with increasing $R > R_c$, that is apparently independent of crack closure, which is the focus of the current work. We examine this behavior in a Ti–6Al–4V alloy processed for turbine blade applications, and consider possible mechanistic explanations.

2. Background

The progressive downward trend of the threshold ΔK_{th} with increasing load ratio at $R > R_c$ was noted by Döker [12] based on the fatigue study of Huthmann and Gossmann [13] on a high-temperature steel at 550°C. Döker chose to characterize this behavior with an empirical relationship, which varied linearly with K_{max}:

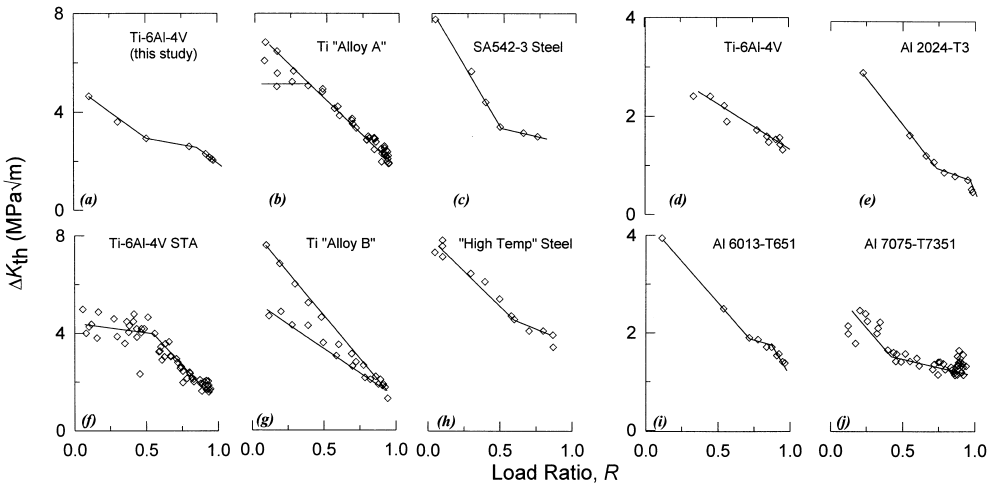

Fig. 2. A representative sampling of large data sets on the influence of load ratio on the fatigue threshold, ΔK_{th}. Rather arbitrary lines are drawn through the data as a guide to interpretation. The only consistent trend among the various curves is that all slopes tend to be $\leqslant 0$. The slopes continue to be $\leqslant 0$ even at high load ratios, where closure has presumably been eliminated. These data sets are taken from (clockwise from upper left): this study, Refs. [1], [10,11], [13–17].

$$\Delta K_{th} = \Delta K_{th,0} + \alpha K_{max}, \quad \text{if } R > R_c, \tag{2}$$

where $\Delta K_{th,0}$ is the ΔK_{th}-intercept extrapolated to $K_{max} = 0$ and α is the slope of the decrease in threshold with increasing K_{max}. The work of Bray and Donald [14] on Al alloys also noted a decrease in ΔK_{th} which is apparently independent of crack closure, although in this case the behavior was parameterized by a power-law relationship:

$$\Delta K_{th} = c(K_{max})^{d}, \quad \text{if } R > R_c. \tag{3}$$

Whereas only a few studies have parameterized (or even noted) this behavior, many published data sets exhibit a similar trend (for examples, see Refs. [1,11,13–19]), most notably the actual data of Schmidt and Paris (Fig. 2e). To examine this effect further, a literature survey was conducted to identify published data sets on steels, aluminum and titanium alloys that contain high load-ratio threshold data. Data sets containing at least three threshold conditions where $K_{max} \geqslant 10$ MPa$\sqrt{\text{m}}$ were regressed according to a normal linear model. To exclude the effects of crack closure, the regression was only performed on those data points where $K_{max} \geqslant 10$ MPa$\sqrt{\text{m}}$. The results of this analysis are presented in Table 1.

In Table 1, all titanium alloys have a negative value for α in the range of -0.01 to -0.07 (this excludes the value of α of -0.386 that is presumably skewed due to the small number of data points and has a large standard deviation of 0.239). Furthermore, for eight of the 10 titanium data sets, a hypothesis that $\alpha = 0$ is rejected based on a 99% confidence interval. This is not the case for all of the steel data sets and two of the three aluminum data sets, where the hypothesis that $\alpha = 0$ is not rejected based on a 99% confidence interval. This indicates that in the case of aluminum or steels, there is not enough statistical evidence to determine that the threshold changes with increasing K_{max}. However, in the case of the titanium data sets, the decrease in threshold with increasing K_{max} is statistically significant. Such behavior is inconsistent with the notion that (global) crack closure is the only mechanism responsible for the R and K_{max} effects on ΔK_{th}.

Table 1
Values for the slope, α, of ΔK_{th} versus K_{max} when $K_{max} \geqslant 10$ MPa$\sqrt{m}$

Material	Temp. (°C)	Method	N[a]	K_{max} range (MPa$\sqrt{m}$)	α	SD(α)[b]	References
Steels:							
High-temp steel	550°C	Const-R	4	10–21	−0.141	0.091	[13]
		Const-K_{max}	4	11–30	−0.044	0.029	[13]
Steel 42CrMo4	RT[c]	Const-K_{max}	8	13–50	−0.005	0.007	[16]
		Jump III[d]	21	12–35	−0.001	0.006	[16]
Aluminum Alloys:							
Al 2024 T3	RT[c]	Const-R	3	15–31	−0.016	0.010	[1]
Al 6013-T651	RT[c]	Const-K_{max}	6	10–38	−0.013	0.006	[14]
Al 7075-T7351	RT[c]	Const-K_{max}	10	12–21	+0.017	0.019	[17]
Titanium Alloys:							
Ti Alloy A	RT[c]	Const-R	12	10–32	−0.063	0.027	[18]
		Const-K_{max}	17	12–40	−0.043	0.012	[18]
Ti Alloy B	RT[c]	Const-K_{max}	11	10–24	−0.062	0.023	[18]
Ti–6Al–4V STA	RT[c]	Const-R	4	10–14	−0.386	0.239	[17]
		Const-K_{max}	18	10–32	−0.024	0.009	[17]
Ti–6Al–4V	RT[c]	Const-K_{max}	3	13–25	−0.050	0.025	[16]
		Jump III[d]	3	13–25	−0.069	0.035	[16]
		Jump IV[d]	3	13–25	−0.063	0.032	[16]
Ti–6Al–4V	RT[c]	Const-K_{max}	4	10–25	−0.011	0.007	[19]
Ti–6Al–4V STOA	RT[c]	Const-R, K_{max}	5	13–57	−0.013	0.006	This study

[a] Number of data points used for regression.
[b] Standard deviation of the slope parameter, α.
[c] Room temperature.
[d] For an explanation of these "jump-in" threshold-determination methods, see Ref. [16].

In the absence of closure, possible alternative mechanisms for this behavior include the presence of sustained-load cracking (SLC) mechanisms, such as creep or hydride-assisted cracking, or the occurrence of the so-called "Marci effect", as described below. Both of these phenomena have been observed in titanium alloys at ambient temperatures.

Sustained-load cracking: It is well established that many titanium alloys exhibit stable crack growth under monotonic loading when the applied K exceeds a sustained-load cracking (SLC) threshold yet is less than K_{Ic} (for a review, see Ref. [20]). In Ti–6Al–4V, it has been noted that such SLC rates increase with increasing internal hydrogen content. Furthermore, SLC rates have been found to vary with temperature. For an alloy containing 50–70 ppm H, crack velocities were at a maximum at ~0°C ($da/dt \sim 5 \times 10^{-10}$ m/s) whereas below −10°C or above 25°C, crack velocities were much slower ($da/dt < 1 \times 10^{-11}$ m/s) [21]. The occurrence of such mechanisms during near-threshold fatigue-crack growth would impart an influence of K_{max} on the threshold and growth-rate behavior as they are primarily controlled by the static, rather than cyclic, loads.

The Marci effect: Some titanium alloys exhibit the so-called "Marci effect" at very high K_{max} levels. In these instances, the fatigue threshold ceases to exist and at all applied ΔK levels (including static loading, where $\Delta K = 0$), the crack advances with a substantial velocity, typically $>10^{-8}$ m/cycle (Fig. 3). This behavior has been observed by Marci on Ti–6Al–6V–2Sn, IMI 834, IMI 685 [22,23], and by Lang on Ti–6Al–2Sn–4Zr–6Mo [24], and is likely associated with SLC. It is possible that this effect is a more aggressive example of the current observations, although there is no evidence to date that conclusively connects these two phenomena.

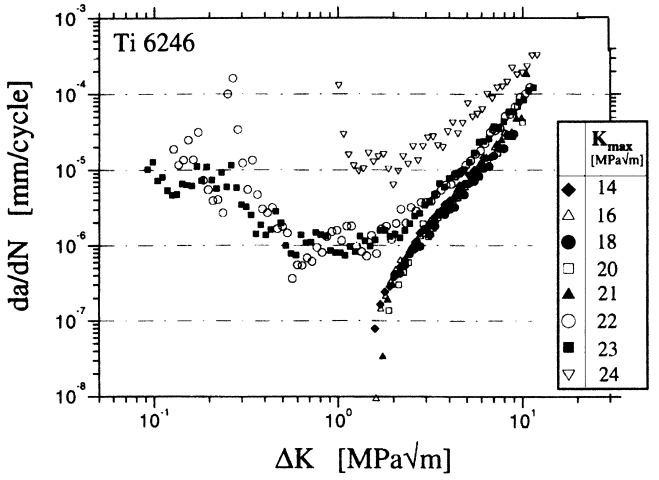

Fig. 3. Fatigue-crack growth behavior typical of the "Marci" effect in Ti–6Al–2Sn–4Zr–6Mo. In some titanium alloys, when K_{max} is greater than some critical value (21 MPa$\sqrt{m}$ in this particular alloy), the fatigue threshold ceases to exist and all applied ΔK values lead to an appreciable growth rates $>10^{-10}$ m/cycle (after Ref. [24]).

3. Experimental procedures

3.1. Material

The material under investigation was a Ti–6Al–4V alloy with a composition (in wt.%) of 6.30Al, 4.17V, 0.19Fe, 0.19O, 0.013N, 0.0035H, balance Ti. It was received as 20 mm thick forged plates from Teledyne Titanium after solution treating 1 h at 925°C and vacuum annealing for 2 h at 700°C. This alloy, which has been chosen as the basis of a comprehensive military/industry/university program on *High Cycle Fatigue*, has a microstructure consisting of a bimodal distribution of ~60 vol% primary-α and ~40 vol% lamellar colonies of $\alpha + \beta$ (Fig. 4). [2] This microstructure displays room temperature yield and tensile strengths of 930 and 970 MPa, respectively, and a Young's modulus of 116 GPa [25]. The fracture toughness, K_{Ic}, was measured to be ~67 MPa$\sqrt{m}$.

3.2. Crack-propagation testing

3.2.1. Cyclic fatigue

Fatigue-crack propagation studies were conducted on large (>10 mm) through-thickness cracks in compact-tension C(T) specimens (L–T orientation; 8 mm thick, 25 mm wide) cycled at load ratios varying from 0.10 to 0.95 in a laboratory air environment (22–32°C, [3] ~45% relative humidity). To approach the threshold, both constant-R and constant-K_{max} loading regimens were employed. Under both conditions, the cyclic stress intensity was varied according to the relationship:

[2] In the context of the Air Force *High Cycle Fatigue* program, this microstructure in Ti–6Al–4V has been referred to as "solution treated and overaged" (STOA).

[3] For fatigue testing at 1000 Hz, the average temperature of the sample rises ~10°C over ambient conditions.

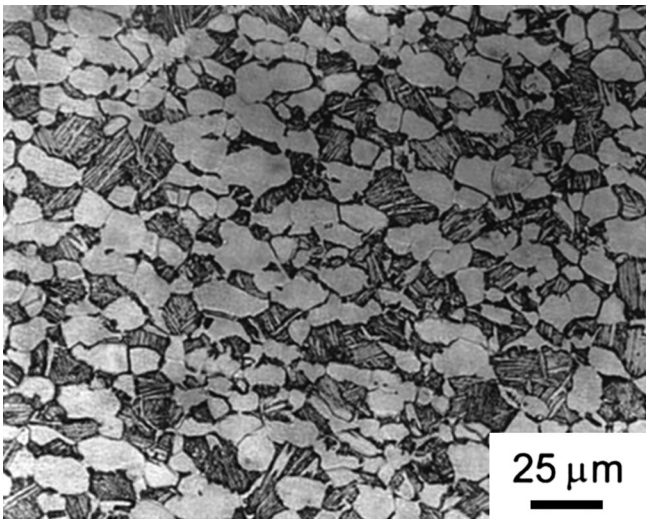

Fig. 4. Ti–6Al–4V in the "STOA" microstructure consisting of a bimodal distribution of ~60 vol% primary-α and ~40 vol% lamellar $\alpha + \beta$. This microstructure was chosen as the basis for a joint military/industry/university program on high cycle fatigue.

$$\Delta K = \Delta K_{\text{initial}} \exp\left[C(a - a_{\text{initial}})\right], \tag{4}$$

where a_{initial} and a are the initial and current values of the crack length, respectively, $\Delta K_{\text{initial}}$ is the initial value of ΔK, and C is the normalized K-gradient, set to a value of $C = -0.08$ mm^{-1} (as suggested in ASTM Standard E-647). Constant-$K_{\max}$ tests were employed to achieve threshold values at very high load ratios, i.e., $R > 0.8$, thereby minimizing the effects of crack closure and representing worst-case *in-service* load ratios [26,27]. Loading frequencies were varied between 50 and 1000 Hz (sine wave). At 50–200 Hz, testing was conducted on conventional servo-hydraulic testing machines operating under automated closed-loop K control; corresponding tests at 1000 Hz were performed under K control on newly developed MTS servo-hydraulic test frames using voice-coil servovalves. The values of the fatigue thresholds, ΔK_{th} and $K_{\max,\text{th}}$, were defined as the minimum values of these parameters yielding a propagation rate of 10^{-10} m/cycle. Crack lengths were monitored in situ using back-face strain compliance techniques, with measurements verified periodically by optical inspection. Crack closure was also monitored using back-face strain compliance; specifically, the global closure stress intensity, K_{cl}, was obtained from the closure load, P_{cl}, which was approximated as the point of first deviation from linearity in the elastic compliance curve upon unloading [28], similar to the method described by Elber [29]. Based on such measurements, an effective (near-tip) stress-intensity range, $\Delta K_{\text{eff}} = K_{\max} - K_{\text{cl}}$, was estimated.

3.2.2. Sustained-load cracking

SLC experiments were conducted using similar methodology to that for fatigue-crack growth. A pre-crack was grown under constant-$K_{\max}$ fatigue loading conditions, with the $K_{\max}$ of the fatigue precrack chosen to equal the post-fatigue sustained-K, K_{SLC}. During precracking, ΔK was shed according to Eq. (4) until a threshold growth rate of $\sim 10^{-10}$ m/cycle was reached. The ΔK level was then reduced to 0.3–0.5 MPa$\sqrt{\text{m}}$ while holding $K_{\max}$ constant. This small ΔK-cycle was chosen to be considerably smaller than the fatigue threshold (~2 MPa$\sqrt{\text{m}}$) while retaining sufficient amplitude to facilitate "sustained-load" growth monitoring via back-face strain compliance, as had been used in the prior fatigue loading.

4. Results

4.1. Effect of loading frequency

A comparison of fatigue-crack propagation behavior at 50 and 1000 Hz is shown in Fig. 5 for load ratios of $R = 0.1$ and 0.8. Similar observations were made under constant-K_{max} loading conditions at $K_{max} = 36.5$ and 56.5 MPa$\sqrt{m}$ ($R \approx 0.9$ and 0.95 respectively). At all observed load ratios, a change in frequency induced a negligible (typically < 0.1 MPa$\sqrt{m}$) change in the ΔK level for a given growth rate, well within the experimental scatter and specimen-to specimen variation. Additional data obtained on the same alloy and microstructure at ~1700 [30] and 20,000 Hz [31] also shows no significant frequency effect on the near-threshold fatigue behavior (Fig. 6). Such frequency-independent growth rates for titanium alloys tested in air have also been reported for the 0.1–50 Hz range [33,34]; the current work extends this observation beyond 1000 Hz.

4.2. Effect of load ratio

Fatigue-crack propagation data collected under constant-R loading conditions are shown in Fig. 7 at four load ratios: $R = 0.1$, 0.3, 0.5, and 0.8 (50 Hz). These results are compared to constant-K_{max} fatigue-crack propagation at four K_{max} values: $K_{max} = 26.5$, 36.5, 46.5, and 56.5 MPa$\sqrt{m}$ (1000 Hz) in Fig. 8. As expected, higher load ratios result in lower ΔK_{th} thresholds and faster growth rates at a given applied ΔK value. Furthermore, this particular alloy does not exhibit the "Marci" effect as described previously. In Table 2, a comparison is given of the ΔK levels required to achieve a growth rate (da/dN) of 10^{-9} and 10^{-10} m/cycle (the latter representing the threshold ΔK_{th}) for all eight loading conditions. These results are compiled in Fig. 9a and b where the measured variation of the ΔK_{th} and $K_{max,th}$ thresholds with positive R are compared.

The role of load ratio at near-threshold levels is generally attributed to crack closure, which is typically associated with the roughness-induced mechanism in titanium alloys [35–37]. In the current experiments,

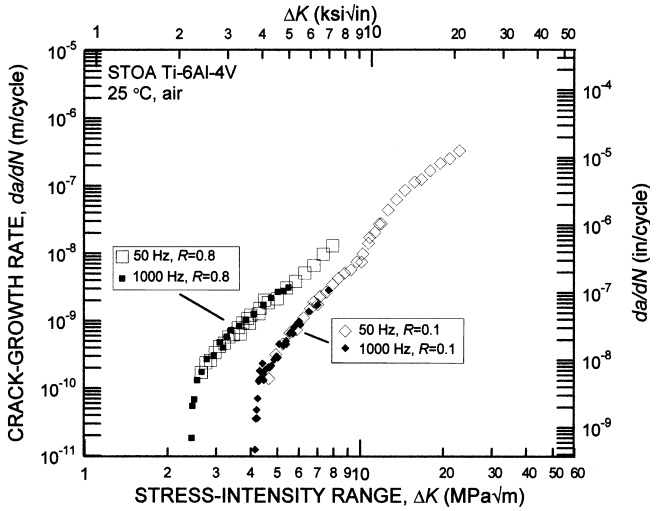

Fig. 5. Fatigue crack growth behavior of bimodal Ti–6Al–4V at two load ratios ($R = 0.1$ and 0.8) and two frequencies ($\nu = 50$ and 1000 Hz) suggesting that there is negligible influence of frequency in near-threshold growth behavior. Similar observations were made under constant-K_{max} loading conditions of $K_{max} = 36.5$ and 56.5 MPa$\sqrt{m}$.

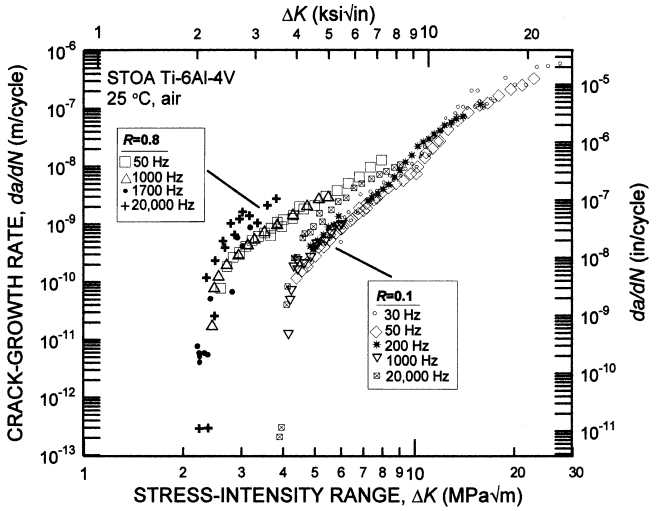

Fig. 6. Fatigue crack growth behavior of bimodal Ti–6Al–4V in the frequency range of 50–20,000 Hz indicating no obvious frequency effect in the near-threshold regime. Data at 1700 Hz were collected using a magnetostrictive fatigue loading stage by Davidson [30]. Data at 20,000 Hz were collected using ultrasonic fatigue by Mayer and Stanzl-Tschegg [31]. Data at 30 Hz was collected by Hines and Lütjering [32].

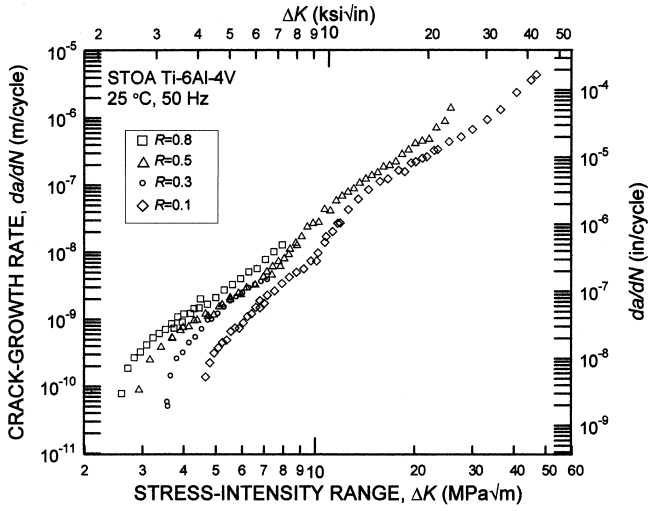

Fig. 7. Effect of load ratio, R, on fatigue crack propagation under constant-R loading. As the load ratio is increased, the growth rates at a given ΔK increase and the fatigue threshold decreases.

closure was approximated from the deviation from linearity in the unloading compliance curve. At low load ratios, $R < 0.5$, closure values were found to be approximately constant at $K_{cl} \sim 2.0$ MPa$\sqrt{m}$, however, no closure was detected at $R > 0.5$. This closure value was essentially identical for $R = 0.1$ and 0.3; moreover, the closure value did not change substantially as ΔK was shed towards threshold. The variation of thresholds, ΔK_{th} and $K_{max,th}$, with load ratio (Fig. 9a and b) show an apparent transition at $R \sim 0.5$, consistent with the Schmidt and Paris [1] analysis (Eq. (1)) which would predict a transition at $R \sim 0.3$–0.5 based on the measured closure value of 2 MPa$\sqrt{m}$. Perhaps the most convincing representation of this

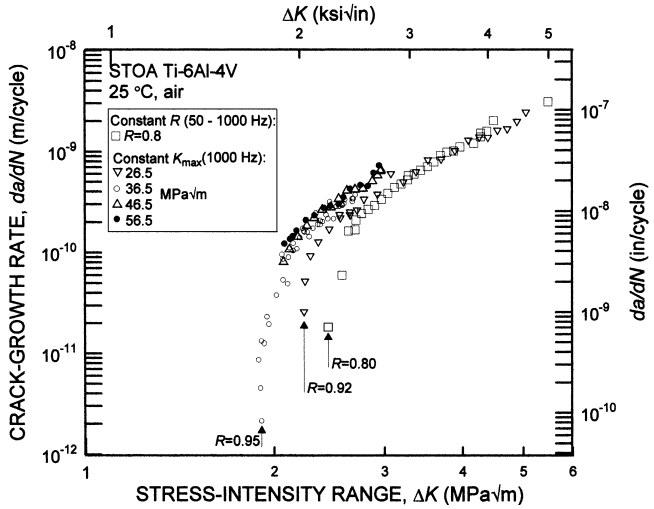

Fig. 8. Fatigue crack propagation data collected under constant-K_{max} conditions compared to $R = 0.8$ data (squares) collected under constant-R conditions. As K_{max} was increased such that the load ratios exceed $R = 0.8$, the value of the fatigue threshold continued to decrease. This decrease in the fatigue threshold with increasing K_{max} is observed in the apparent absence of crack closure, as detected by back-face strain compliance.

Table 2
ΔK levels required for growth rates of 10^{-9} and 10^{-10} m/cycle

R	K_{max} (MPa$\sqrt{m}$)	ΔK (MPa$\sqrt{m}$)
Growth rate, $da/dN = 10^{-9}$ m/cycle		
0.1[a]	6.47–6.92	5.82–6.23
0.3[a]	6.77–6.83	4.74–4.78
0.5[a]	8.66–9.26	4.33–4.63
0.8[a]	18.6–20.2	3.72–4.03
0.85	26.5[a]	3.85
0.90	36.5[a]	~3.6
0.93	46.5[a]	~3.4
0.94	56.5[a]	~3.15
Growth rate, $da/dN = 10^{-10}$ m/cycle		
0.1[a]	4.72–4.78	4.25–4.30
0.3[a]	5.16	3.61
0.5[a]	5.86	2.93
0.8[a]	12.5–13.1	2.50–2.61
0.91	26.5[a]	2.33
0.94	36.5[a]	2.11–2.15
0.955	46.5[a]	2.09
0.954	56.5[a]	~2.04

[a] This value was held constant during the fatigue test.

transition from a "closure-affected" to a "closure-free" threshold is shown in a plot of ΔK_{th} versus $K_{max,th}$ in Fig. 9c, which is simply a coordinate transformation of Fig. 9a and b. The distinct change in slope in Fig. 9c is surely associated with some change in governing mechanism, and is, in this case, coincident with the elimination of global crack closure.

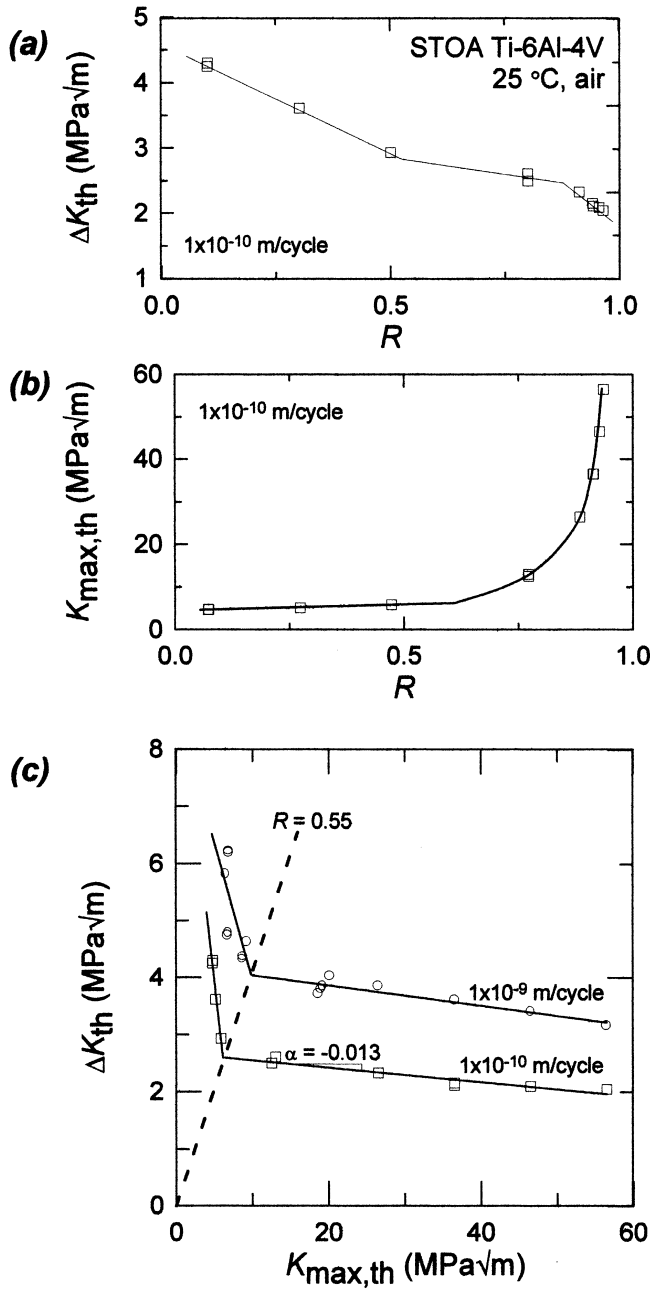

Fig. 9. Loading conditions for a threshold growth rate of 10^{-10} m/cycle in bimodal Ti–6Al–4V (50 Hz and 1000 Hz). (a) Cyclic stress intensity at threshold, ΔK_{th}, as a function of load ratio, R (b) the maximum stress intensity at threshold, $K_{max,th}$, as a function of R. (c) ΔK_{th} as a function of $K_{max,th}$ (along with data collected for a growth rate of 10^{-9} m/cycle). Of the three parameters, ΔK_{th}, $K_{max,th}$, and R, only two are unique.

In the case where crack closure is the only mechanism responsible for the load ratio effect, one might expect that a closure-corrected stress-intensity range, ΔK_{eff}, would yield a crack-propagation curve which is

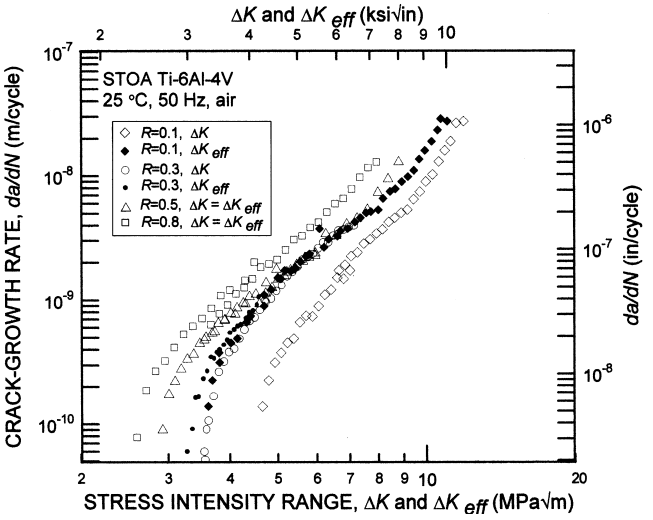

Fig. 10. Considering only 50 Hz, constant-R data, raw growth data (open symbols) is compared to closure corrected data (closed symbols) where closure is assessed by determining the effective stress intensity range: $\Delta K_{\text{eff}} = K_{\max} - K_{\text{cl}}$.

unaffected by load ratio. Indeed, in the current study, ΔK_{eff} does tend to normalize the low load ratio data ($R < 0.5$) onto a single curve (Fig. 10) (see also Ref. [5]). However, above $R \sim 0.5$ where (global) closure was not experimentally detected, ΔK_{th} values continue to decrease with increasing R. This is also apparent in the plot of ΔK_{th} versus $K_{\max,\text{th}}$ in Fig. 9c; in the region where threshold is $K_{\max}$-controlled, ΔK_{th} is not invariant and decreases approximately linearly with increasing $K_{\max}$. The slope of this decrease can be quantified in terms of Eq. (2) as $\alpha = -0.013$, implying that an increase in the $K_{\max}$ value of 10 MPa$\sqrt{\text{m}}$ is associated with a 0.13 MPa$\sqrt{\text{m}}$ decrease in ΔK_{th} threshold.

4.3. Fractography and crack profiles

Fractography (from scanning electron microscopy) and crack profiles (from optical microscopy) corresponding to the threshold growth rate of 10^{-10} m/cycle at three load ratios, $R = 0.1$, 0.5, and 0.95, are compared to the static overload condition in Fig. 11. The crack profiles for the three load ratios show a decrease in crack-path tortuosity as R or $K_{\max}$ is increased. Nevertheless, there are only minimal differences in the fractography for the three different load ratios, even though they span more than an order of magnitude in $K_{\max}$ and two orders of magnitude in the plastic-zone size. There is a clear distinction, however, in the morphology of the fatigue surfaces compared to that of the overload fracture condition where microvoid coalescence can be seen. Thus, it can be concluded that, even at $R = 0.95$ where $K_{\max} = 57$ MPa$\sqrt{\text{m}}$ ($K_{\max}/K_{\text{Ic}} \cong 0.85$), there is no clear evidence of static fracture modes, in this case due to microvoid coalescence, in the fractography of fatigue-crack growth in this alloy.

4.4. Effect of internal hydrogen content

To study the effects of internal hydrogen content, several samples were heat treated in high vacuum at 700°C for 24 h thereby reducing the hydrogen content from an as-received value of ~35 to ~5 ppm with no apparent microstructural changes. The low-hydrogen specimens were subsequently tested under fatigue loading conditions at constant-$R = 0.5$ and constant-$K_{\max} = 28$ MPa$\sqrt{\text{m}}$. A comparison of the near-threshold fatigue-crack growth behavior for the as-received and low internal hydrogen conditions is

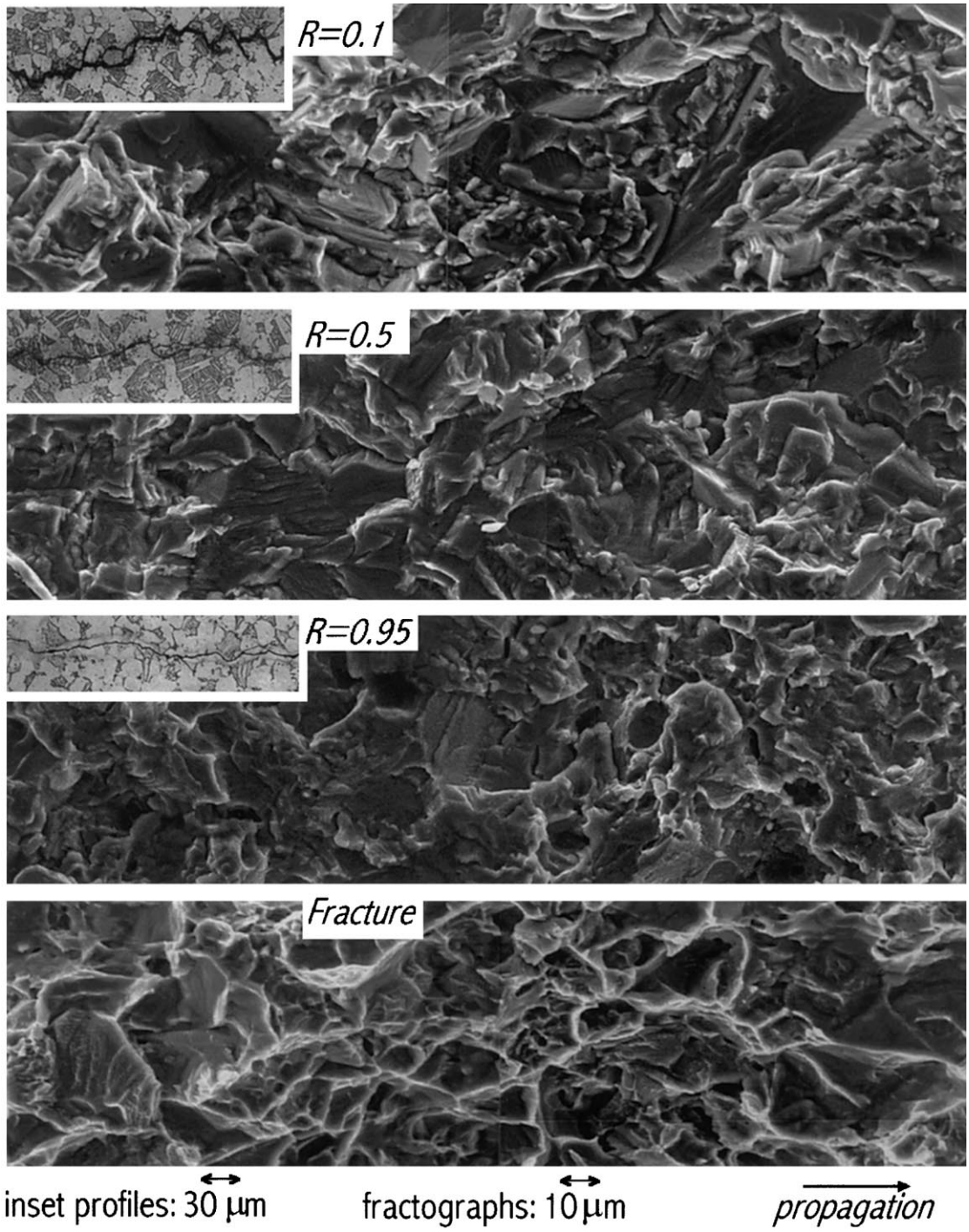

Fig. 11. A comparison of fractography and crack profiles under fatigue (observing a threshold growth rate $\sim 10^{-10}$ m/cycle at three load ratios, $R = 0.1$, 0.5, and 0.95) and static overload fracture condition. While microvoid coalescence is apparent in the overload fracture, there is no clear evidence of this mode in the fatigue fractographs, even at $R = 0.95$ where $K_{max} = 57$ MPa$\sqrt{}$m.

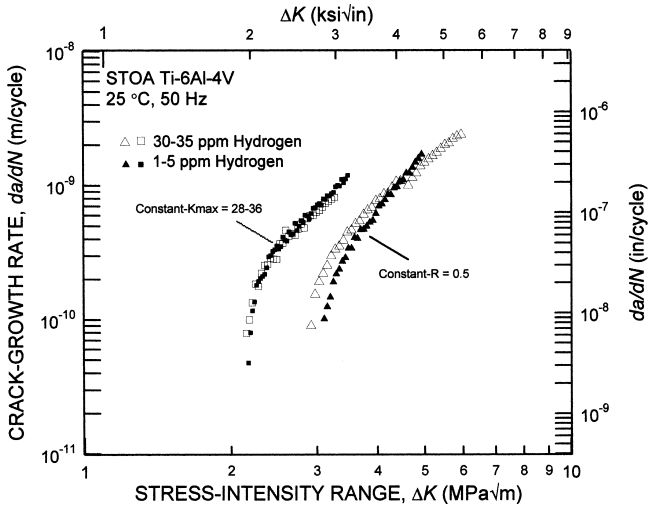

Fig. 12. The effect of internal hydrogen on near-threshold fatigue-crack propagation behavior in bimodal Ti–6Al–4V. Although the hydrogen content was reduced by a factor of six or more, the ΔK_{th} threshold is still significantly affected by load ratios in excess of the "closure-free" transition, $R \sim 0.5$.

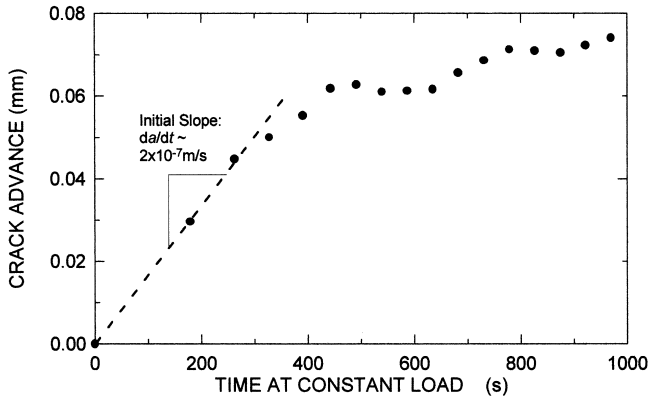

Fig. 13. Transient SLC observed at $K = 36.5$ MPa$\sqrt{}$m. The initial SLC growth-rate of 2×10^{-7} m/s is similar to the difference in the fatigue-crack growth rates between $R = 0.8$ and $K_{max} = 36.5$ MPa$\sqrt{}$m (Fig. 8).

presented in Fig. 12, where it is apparent that there is little effect of hydrogen content (~5–35 ppm) in this alloy. Most specifically, we see that the threshold was still affected by load ratios in excess of the "closure-free" transition ($R > 0.5$), in spite of the very low hydrogen content, and that the extent of this effect appears to be independent of hydrogen content over this range.

4.5. Sustained-load cracking

The results of sustained-load tests on the Ti–6Al–4V alloy at a constant applied stress intensity of $K = 36.5$ MPa$\sqrt{}$m, shown in Fig. 13, indicate approximately 80 μm of slow crack growth over the first 1000 s following initiation from the fatigue pre-crack. The initial growth rate of $\sim 2 \times 10^{-7}$ m/s was seen to decay until crack arrest ($<1 \times 10^{-11}$ m/cycle) within 1000 s. This transient behavior indicates that for

near-threshold fatigue-crack growth to be affected by SLC, then the SLC mechanism must be "restarted" by each fatigue cycle. Without "restarting" on each fatigue cycle, the SLC growth-rate would decay to arrest within the first several minutes of a constant-K_{max} fatigue test, and thus would have little or no effect on the value of the fatigue threshold.

5. Discussion

Crack closure is generally considered to be the primary reason for the effect of load ratio on the ΔK_{th} fatigue threshold in metallic materials. Indeed, at low load ratios such that $R < R_c$, the closure-based analysis describes threshold behavior reasonably well in most cases, including the data presented in this paper. However, based on the closure argument, at load ratios where K_{min} exceeds K_{cl}, (i.e. $R > R_c$) such that the influence of (global) closure is minimized, the value of ΔK_{th} would be expected to become independent of R. This is the generally anticipated behavior, however, in the current Ti–6Al–4V alloy, we have observed a progressive reduction in ΔK_{th} from $R = 0.5$ (the "closure-free" condition) to $R = 0.95$; specifically, a ~ 1 MPa$\sqrt{}$m decrease in ΔK_{th} is found as K_{max} increases from ~ 6 MPa$\sqrt{}$m (at $R = 0.5$) to 57 MPa$\sqrt{}$m (at $R = 0.95$). Furthermore, examples have been given (Table 1) of several other Ti-alloys that also exhibit a K_{max}-sensitivity on the threshold at high load ratios ($R > R_c$).

As noted previously, one possible explanation for this effect is the occurrence of SLC mechanisms during fatigue-crack growth at high load ratios, where the high values of K_{max} exceed some SLC threshold. This being the case, the measured fatigue-crack growth rates would result from contributions from both mechanical fatigue cracking, $(da/dN)_{fatigue}$, and that due to SLC $(da/dt)_{SLC}$, as modeled using a process competition [38] or, as indicated in Eq. (5), a superposition [39] model: [4]

$$\left.\frac{da}{dN}\right|_{total} = \left.\frac{da}{dN}\right|_{fatigue} + \frac{1}{v}\left.\frac{da}{dt}\right|_{SLC}. \tag{5}$$

Support for this notion comes from the observation that the measured sustained-crack growth rate of $\sim 2 \times 10^{-7}$ m/s at a sustained K of 36.5 MPa$\sqrt{}$m corresponds to a growth rate per cycle at 1000 Hz of $\sim 2 \times 10^{-10}$ m/cycle, which is similar to the difference in the fatigue-growth rates at a given applied ΔK for $R = 0.5$ compared to 0.95. Two possible mechanisms for such SLC are described below:

(i) *Stress-assisted hydride formation*. Several independent studies in titanium alloys have concluded that under sufficient triaxial stress, internal hydrogen can precipitate as metal hydrides at α/β [40] or α/α [41] interfaces, or within α-grains [20] leading to brittle fracture of the hydrides. This phenomenon has been used to explain both sustained-load cracking [20,21,42], where crack advance is observed under monotonic load, and accelerated fatigue-crack propagation at high load ratios [40,43].

(ii) *Creep-assisted crack growth*. Alternatively, since room-temperature creep can occur in titanium alloys, it has been suggested that the role of hydrogen is to accelerate SLC by creep rather than through hydride formation. Williams [44], for example, observed in Ti–6Al–4V that the threshold stress intensity for failure by SLC, $K_{SLC,th}$, increased with increasing hydrogen content, which is apparently counterintuitive to the hydride formation mechanism. Furthermore, second-stage creep rate was observed to decrease significantly with increasing hydrogen content; at 95% of the yield strength, the creep rate decreased from 120×10^{-6} %/h for 7 ppm H to 36×10^{-6} %/h for 60 ppm H. From these or similar observations, some authors [44,45] have concluded that the role of hydrogen in sustained load crack stems from creep behavior rather than the formation and failure of brittle hydrides.

[4] One might argue that these models may be overly simplistic. Nevertheless, the rather basic notion that mechanical fatigue and SLC should somehow act in concert is what is most important for the ensuing arguments.

Both of the aforementioned mechanisms suggest that the degree and extent of SLC is related to the internal hydrogen content, although the exact role of hydrogen is still controversial. Nevertheless, if SLC growth was a significant contribution to the observed fatigue crack-growth rates at high load ratios, one may expect that the high-R behavior could be altered by changing the internal hydrogen content. Alternatively, if hydrogen could (hypothetically) be entirely removed, the SLC mechanism should be entirely eliminated, thereby yielding an invariant ΔK_{th} threshold above the "closure-free" transition ($R > 0.5$), assuming that there are no *additional* mechanisms present. However, as illustrated in Fig. 12, a reduction in the hydrogen content by more than a factor of six has essentially no effect on the fatigue thresholds in this alloy. Moreover, the K_{max}-sensitivity of the fatigue threshold at high load ratios remains essentially unchanged by the reduction in internal hydrogen.

Furthermore, setting the hydrogen observations aside, it seems unlikely that any SLC mechanism could provide a major contribution to fatigue in this alloy in light of the observed frequency independence ($v = 50$–1000 Hz) of fatigue-crack propagation that is observed at all load ratios (Fig. 6). Indeed, the observed frequency independence indicates that if a chemically- or electrochemically-controlled mechanism was related to the observed high-R load ratio effect, then the time-dependent processes must go to completion within 1 ms (the time for one cycle at 1000 Hz).

Finally, any thermally-activated mechanism such as SLC, would be expected to manifest itself in the temperature dependence of fatigue behavior. Thomas [46] has observed the SLC and fatigue-crack growth at three temperatures (−30°C, 22°C and 140°C) in the same alloy and microstructure considered in this study. He found that the extent of SLC transient growth decreased with increasing temperature, obeying an Arrhenius relationship. At a sustained K of 60 MPa$\sqrt{}$m, there was ~500 μm of transient growth at −30°C, but only ~45 μm of such growth at 140°C. Therefore, for SLC to be an important component of this alloy's fatigue behavior, one may expect the fatigue behavior to also be temperature-dependent. However, over this same range in temperature, the fatigue behavior of this alloy remained invariant (observed at $K_{max} =$ 60 MPa$\sqrt{}$m).

While there is no doubt that SLC does occur in many titanium alloys, the observed lack of an effect of frequency, temperature, or hydrogen content on fatigue behavior strongly suggest that SLC does not contribute significantly to the K_{max}-sensitive fatigue behavior at high load ratios in this particular alloy and microstructure. However, since the slopes, α, of ΔK_{th} versus K_{max} (for $R > R_c$) relationship (Eq. (1)) vary by a factor of roughly seven in titanium alloys and the current alloy/microstructure is at the shallow end of this range, it is conceivable that SLC does contribute to fatigue-crack growth behavior in certain other Ti alloy microstructures, particularly those with higher internal hydrogen content. Indeed, there is some evidence in the literature that SLC may be an important component in the high-R fatigue behavior of *other* titanium alloys. For example, Pao et al. [40] studied the effect of hydrogen content on the fatigue threshold of a β titanium alloy at $R = 0.9$. As might be expected from a SLC contribution, they observed the fatigue threshold to decrease with increasing hydrogen content. Specifically, when the hydrogen content was changed from 40 to 1000 ppm, the threshold was reduced from 2.7 to 2.0 MPa$\sqrt{}$m. This is in contrast to the behavior currently observed in the $\alpha + \beta$ alloy in this study where an increase in hydrogen content from ~5 to ~35 ppm did not alter the threshold (Fig. 12), albeit these two observations were over different ranges of hydrogen content.

As the observed lack of a significant frequency or temperature effect on fatigue-crack propagation in this alloy largely negates a major role of environmentally-assisted mechanisms in influencing the K_{max} dependence of the ΔK_{th} threshold, other purely mechanical mechanisms may be considered, as described below.

(i) Microscopic near-tip closure. During in situ studies in the scanning electron microscope of fatigue-crack propagation behavior in the same titanium alloy and microstructure at >1000 Hz, Davidson reported that he detected crack closure in the local region (within ~10 μm) behind the crack tip, despite being at R

values of 0.8–0.9, i.e., well above the (global) "closure-free" load ratio, R_c [30]. While this near-tip (or local) closure is essentially undetectable by the macroscopic techniques such as unloading compliance, it could nevertheless significantly affect the effective stress intensity experienced at the crack tip. In this way, closure would exist at all load ratios; however, the extent of the crack flank over which it operates would be a function of the load ratio (or more specifically, the minimum stress intensity). However, what detracts from this explanation is the marked transition at $R = 0.5$. As shown in Fig. 9c, there is a distinct transition from ΔK-controlled to K_{max}-controlled thresholds at $R = 0.5$. It is difficult to reconcile this observation with a near-tip closure model, which would presumably manifest itself in a smooth transition from global- to near-tip closure as the extent of the closure wake grew smaller.

(ii) Static fracture modes. As K_{max} values approach the point of instability, as characterized by K_{Ic}, additional *static* fracture modes, specifically cleavage, intergranular fracture or void coalescence, can occur during fatigue-crack growth and lead to accelerated growth rates and a strong sensitivity to both load ratio and K_{max} [9]. Such behavior is most often observed at lower load ratios and high growth rates, e.g. $>10^{-5}$ m/cycle, where the ΔK level is large such that $K_{max} \rightarrow K_{Ic}$; in the present work at high load ratios where K_{max} is held near K_{Ic}, static fracture modes could presumably occur even at near-threshold growth rates. The occurrence of such static modes provides a very feasible explanation of the continued K_{max}-dependency of fatigue behavior at load ratios above the "closure-free" condition, R_c. However, scanning electron micrographs of the fatigue fracture surfaces, shown in Fig. 11, reveal no such differences in the near-threshold fracture morphology at $R = 0.5$ and 0.95, despite the order of magnitude increase in K_{max} (threshold K_{max} values are 5.9 and 56.5 MPa$\sqrt{m}$ at $R = 0.5$ and 0.95, respectively). Furthermore, the mechanism responsible for the downward trend in ΔK_{th} with increasing R (or K_{max}) appears to active at even moderate "closure-free" load ratios ($R = 0.8$), where K_{max} is much less than K_{Ic}. Based on the lack of apparent static modes in the high-K_{max} fractography, and the observed K_{max}-sensitivity at even moderate load ratios, the static mode argument can be discounted as a potential explanation in this alloy.

(iii) K_{max}-dependence on intrinsic near-threshold fatigue. As noted above, the mechanistic role of R or K_{max} on fatigue-crack growth is traditionally associated with crack closure and/or the occurrence of additional K_{max}-controlled mechanisms, such as environmentally-assisted cracking or static modes. However, these mechanisms do not appear to be the controlling factors in the present alloy at $R > R_c$. Therefore, we must consider whether the magnitude of K_{max} can also affect the *intrinsic* mechanism of fatigue-crack growth, particularly since between $R = 0.5$ and 0.95 where the ΔK_{th} threshold is reduced by $\sim$1 MPa$\sqrt{m}$, the maximum plane-strain plastic-zone size varies by some two orders of magnitude, from $\sim$2 to 200 μm, as K_{max} increases from $\sim$6 to 57 MPa$\sqrt{m}$. Based on this significant change in the local plasticity, it would seem likely that there would be an effect on the fatigue-crack growth behavior and the value of the threshold. However, a majority of the existing *mechanism-based* intrinsic threshold models [47–52], which are most often based on the critical conditions for dislocation emission at the crack-tip, do not explicitly describe the mechanistic nature of a K_{max}-dependent component. The evidence presented here strongly implies that K_{max} does indeed influence the threshold for fatigue-crack growth, independent of crack closure, presumably by its effect on intrinsic crack growth. The precise mechanism of this K_{max} contribution, however, is presently unclear, although mechanisms associated with the spread of local plasticity would appear to be influential. An understanding of this mechanism would greatly enhance our knowledge of the fundamental fatigue process.

6. Conclusions

A study has been made of the role of the maximum stress intensity (K_{max}) and the load ratio (over the range $R = 0.1$–0.95) in influencing fatigue-crack propagation and specifically threshold behavior in a

Ti–6Al–4V alloy, tested over a range of loading frequencies (50–1000 Hz) and in room temperature air (22–32°C, 45% relative humidity). Based on this work, which was focused on an alloy with a bimodal (STOA) microstructure (~60 vol% primary-α, ~40 vol% lamellar $\alpha + \beta$), the following conclusions can be made:

1. Room temperature fatigue-crack growth ($\sim 10^{-12}$–10^{-6} m/cycle) and threshold ΔK_{th} values were found to be independent of loading frequency over the range 50–1000 Hz; companion studies at 20,000 Hz on the same alloy/microstructure, together with previous results in the literature, suggest that such frequency-independent growth rate behavior at near-threshold levels extends over five orders of magnitude from 0.1 to 20,000 Hz.

2. The fatigue thresholds, ΔK_{th} and $K_{max,th}$, were found to vary significantly with positive load ratio ($R = 0.1$–0.95). Consistent with the description of Schmidt and Paris, below a critical load ratio, R_c (~0.5), the $K_{max,th}$ threshold was seen to be independent of R, and the ΔK_{th} decreased with increasing R. By measuring (global) crack closure loads, using unloading compliance techniques, this behavior was found to be consistent with the traditional explanation of load ratio effects on the fatigue threshold involving closure, with R_c defining the condition at which the closure stress intensity, $K_{cl} = K_{min}$.

3. At load ratios larger than R_c, i.e., $R \sim 0.5$–0.95, where (global) crack closure could no longer be detected, a different dependence of the ΔK_{th} threshold on load ratio was seen, with $\Delta K_{th} \to 0$ as $R \to 1$. Such behavior is contrary to conventional explanations of the near-threshold load-ratio effect, which are based on crack closure and imply that ΔK_{th} is independent of load ratio for $R > R_c$. The decrease in ΔK_{th} threshold is approximately linear with increase in K_{max}, decaying at a rate of -0.013. A survey of literature indicated that this effect was seen by several titanium alloys, with slopes varying between -0.01 to -0.07.

4. Explanations for this effect are suggested, based on the occurrence of (i) SLC due to internal hydrogen, (ii) static (K_{max}-controlled) fracture modes, (iii) near-tip crack closure, and (iv) an effect of K_{max} on the intrinsic mechanism of fatigue-crack growth. In the present alloy/microstructure, the effect could not be ascribed to hydrogen-assisted SLC, as fatigue thresholds were unaffected by changes in hydrogen content, frequency, or temperature. Nor was the effect ascribed to the occurrence of static modes, as the morphology of the near-threshold fatigue fracture surfaces was essentially unchanged between load ratios of 0.5–0.95. While near-tip closure may be a source for this effect, it seems most likely that the intrinsic fatigue-crack growth process is itself K_{max} dependent. The K_{max}-sensitivity should be considered in developing mechanistic *intrinsic* threshold models.

Acknowledgements

This work was supported by the US Air Force Office of Scientific Research under Grant No. F49620-96-1-0478 under the auspices of the Multidisciplinary University Research Initiative on *High-Cycle Fatigue* to the University of California. Thanks are due to the Hertz Foundation for a graduate fellowship for B.L.B., to Drs. H.R. Mayer and S.E. Stanzl-Tschegg for performing the ultrasonic fatigue experiments, and to Dr. J.P. Campbell and Z. Bell for experimental assistance.

References

[1] Schmidt RA, Paris PC. Threshold for fatigue crack propagation and the effects of load ratio and frequency. Progress in Flaw Growth and Fracture Toughness Testing, ASTM STP 536, ASTM, Philadelphia, 1973. p. 79–94.

[2] Ritchie RO. Near-threshold fatigue crack propagation in ultra-high strength steel: influence of load ratio and cyclic strength. J Engng Mat Tech ASME Series H 1977;99:195–204.

[3] Liaw PK, Leax TR, Logsdon WA. Near-threshold fatigue crack growth behavior in metals. Acta Metall 1983;31:1581–7.
[4] Taylor D. A compendium of fatigue thresholds and growth rates. Engineering Materials Advisory Services Ltd., West Midlands, UK, 1985.
[5] Dubey S, Soboyejo ABO, Soboyejo WO. An investigation of the effects of stress ratio and crack closure on the micromechanisms of fatigue crack growth in Ti–6Al–4V. Acta Materialia 1997;45:2777–87.
[6] Ritchie RO, Boyce BL, Campbell JP, Roder O, Thompson AW, Milligan WW. Thresholds for high cycle fatigue in a turbine engine Ti–6Al–4V alloy. Int J Fatigue 1999;22:621–31.
[7] Kardomateas GA, Carlson RL. Predicting the effects of load ratio on the fatigue crack growth rate and fatigue threshold. Fatigue Fract Engng Mat Struct 1998;21:411–23.
[8] Chiang CR. Threshold stress intensity factor of fatigue cracks. Engng Fract Mech 1994;49:29–33.
[9] Ritchie RO, Knott JF. Mechanisms of fatigue crack growth in low alloy steel. Acta Metall 1973;21:639–48.
[10] Suresh S, Ritchie RO. On the influence of environment on the load ratio dependence of fatigue threshold in pressure vessel steel. Engng Fract Mech 1983;18:785–800.
[11] Lenets YN, Nicholas T. Load history dependence of fatigue crack growth thresholds for a Ti alloy. Engng Fract Mech 1998;60:187–203.
[12] Döker H. Fatigue crack growth threshold: implications, determination and data evaluation. Int J Fatigue 1997;19:S145–149.
[13] Huthmann H, Gossmann O. Verband für Materialforschung und – prüfung. in 23. Vortragsveranstaltung des DVM-Arbeitskreises Bruchvorgänge, Deutscher, Berlin, 1981. p. 271–84.
[14] Bray GH, Donald JK. Separating the influence of K_{max} from closure-related stress ratio effects using the adjusted compliance ratio technique. In: McClung RC, Newman Jr JC, editors. Advances in fatigue crack closure measurement and analysis: second volume. ASTM STP 1343, American Society for Testing and Materials, Philadelphia, PA, 1997.
[15] Smith SW, Piascik RS. An indirect technique for determining closure free fatigue crack growth behavior. In: Newman JC, Piascik RS, editors. Fatigue crack growth thresholds, endurance limits and design, ASTM STP 1372, American Society for Testing and Materials, Philadelphia, 2000. p. 109–22.
[16] Marci G. A fatigue crack growth threshold. Engng Fract Mech 1992;41:367–85.
[17] Marci G. Non-propagation conditions (ΔK_{th}) and fatigue crack propagation threshold (ΔK_T). Fatigue Fract Engng Mater Struct 1994;17:891–907.
[18] Marci G. Comparison of fatigue crack propagation thresholds of two Ti tubrine-disk materials. Fatigue 1994;16:409–12.
[19] Marci G, Castro DE, Bachmann V. Fatigue crack propagation threshold. J Test Eval 1989;17:28–39.
[20] Moody NR, Costa JE. A review of microstructure effects on hydrogen-induced sustained load cracking in structural titanium alloys. In: Kim Y-W, Bloyer RR, editors. Microstructure/property relationships in titanium aluminides and alloys. The Minerals, Metals, and Materials Society, Warrendale, PA, 1991.
[21] Boyer RR, Spurr WF. Characteristics of sustained-load cracking and hydrogen effects in Ti–6Al–4V. Metall Trans A 1978;9A:23–9.
[22] Marci G. Failure mode below 390 K with IMI 834. In: Lütjering G, Newack H, editors. Fatigue '96. Proceedings of the Sixth International Fatigue Conference, Berlin, Germany, vol. 1, Pergamon, Oxford. 1996. p. 493–8.
[23] Marci G. Werkstofftech. Mat.-wiss 1997;28:51.
[24] Lang M, Hartman GA, Larsen JM. Investigation of an abnormality in fatigue crack growth curves – the Marci effect. Scripta Materialia 1998;38:1803–10.
[25] Eylon D. Summary of the available information on the processing of the Ti–6Al–4V HCF/LCF program plates. University of Dayton Report, Dayton, OH, 1998.
[26] Döker H, Bachmann V, Marci G. A comparison of different methods of determination of the threshold for fatigue crack propagation. In: Bäcklund J, Blom AF, Beevers CJ, editors. Fatigue Thresholds, vol. 1. EMAS, Warley, UK, 1982. p. 45–58.
[27] Herman WA, Hertzberg RW, Jaccard R. A simplified laboratory approach for the prediction of short crack behavior in engineering structures. Fatigue Fract Engng Mater Struct 1988;11:303–20.
[28] Ritchie RO, Yu W. Short crack effects in fatigue: a consequence of crack tip shielding. In: Ritchie RO, Lankford J, editors. Short Fatigue Cracks, TMS, Warrendale, PA, 1986. p. 167–89.
[29] Elber W. Fatigue crack closure under cyclic tension. Engng Fract Mech 1970;2:37–45.
[30] Davidson D. Damage mechanisms in high cycle fatigue. AFOSR Final Report, Project 06–8243. Southwest Research Institute, San Antonio, TX, 1998.
[31] Mayer HR, Stanzl-Tschegg SE. Universität für Bodenkultur, private communication, 1998.
[32] Hines JA, Lütjering G. Propagation of microcracks at stress amplitudes below the conventional fatigue limit in Ti–6Al–4V. Fatigue Fract Engng Mater Struct 1999;22:657–65.
[33] Wanhill RJH. Environment and frequency effects during fatigue crack propagation in Ti–2.5 Cu (IMI 230) sheet at room temperature. Corrosion-NACE 1974;30:28–35.
[34] Dawson DB, Pelloux RMN. Corrosion fatigue crack growth of titanium alloys in aqueous environments. Metall Trans 1974;5:723–31.

[35] Halliday MD, Beevers CJ. Some aspects of fatigue crack closure in two contrasting titanium alloys. J Test Eval 1981;9:195–201.
[36] Ravichandran KS. Near threshold fatigue crack growth behavior of a titanium alloy: Ti–6Al–4V. Acta Metallurgica et Materialia 1991;39:401–10.
[37] Ogawa T, Tokaji K, Ohya K. The effect of microstructure and fracture surface roughness on fatigue crack propagation in a Ti–6Al–4V alloy. Fatigue Fract Engng Mater Struct 1993;16:973–82.
[38] Austen IM, McIntyre P. Corrosion fatigue of high-strength steel in low-pressure hydrogen gas. Metal Sci 1979;13:420–8.
[39] Wei RP, Landes JD. Correlation between sustained-load and fatigue crack growth in high strength steels. Mater Res Standard 1970;9:25–46.
[40] Pao PS, Feng CR, Gill SJ. Hydrogen-assisted fatigue crack growth in beta-annealed Ti–6Al–4V. Scripta Materialia 1998;40:19–26.
[41] Peterson KA, Schwanebeck JC, Gerberich WW. In situ scanning Auger analysis of hydrogen-induced fracture in Ti–6Al–6V–2Sn. Metall Trans A 1978;9A:1169–72.
[42] Sastry SM, Lederich RJ, Rath BB. Subcritical crack-growth under sustained load in Ti–6Al–6V–2Sn. Metall Trans A 1981;12A:83–94.
[43] Pao PS, O'Neal JE. Hydrogen-enhanced fatigue crack growth in Ti–6242S. J Nucl Mater 1984;123:1587–91.
[44] Williams DN. Effects of hydrogen in titanium alloys on subcritical crack growth under sustained load. Mater Sci Engng 1976;24:53–63.
[45] Freed AD, Sandor BI. Localised time-dependent and cycle dependent creep in notched plates. In: Gittus J, editor. Cavities and cracks in creep and fatigue. Applied Science, UK, 1981. p. 89–108.
[46] Thomas JP. Subcritical crack growth of Ti–6Al–4V in the ripple-loading regime. In: Warren JR, Henderson J, editors. Proceedings of the 4th National Turbine Engine High Cycle Fatigue Conference, Monterey, CA, Universal Technology Corp., Dayton, OH, CD-Rom, session 2, 1999. p. 50–60.
[47] Weiss V, Lal DN. A note on the threshold condition for fatigue crack propagation. Metall Trans 1974;5:1946–9.
[48] Sandananda K, Shahinian PP. Prediction of threshold stress intensity for fatigue crack growth using a dislocation model. Int J Fract 1977;13:585–94.
[49] Fine ME. Fatigue resistance of metals. Metall Trans 1980;11A:365–79.
[50] Liu HW, Liu D. Near threshold fatigue crack growth behavior. Scripta Metall 1982;16:595–600.
[51] Weertman J. Fatigue crack growth in ductile metals. In: Mura T, editor. Mechanics of fatigue, AMD-vol. 47. New York: ASME; 1982. p. 11–9.
[52] Davidson DL. A model for fatigue crack advance based on crack tip metallurgical and mechanics parameters. Acta Metall 1984;32:707–14.